Phys Chem Minerals (2006) 33: 192–199
DOI 10.1007/s00269-006-0073-2

ORIGINAL PAPER

C. M. Holl · J. R. Smyth · M. H. Manghnani
G. M. Amulele · M. Sekar · D. J. Frost
V. B. Prakapenka · G. Shen

Crystal structure and compression of an iron-bearing Phase A to 33 GPa

Received: 16 August 2005 / Accepted: 31 January 2006 / Published online: 9 March 2006

Abstract Fe-bearing dense hydrous magnesium silicate Phase A, $Mg_{6.85}Fe_{0.14}Si_{2.00}O_8(OH)_6$ has been studied by single-crystal X-ray diffraction at ambient conditions and by high-pressure powder diffraction using synchrotron radiation to 33 GPa. Unit cell parameters at room temperature and pressure from single crystal diffraction are $a = 7.8678$ (4) Å, $c = 9.5771$ (5) Å, and $V = 513.43$ (4) Å^3. Fitting of the P–V data to a third-order Birch-Murnaghan isothermal equation of state yields $V_0 = 512.3$ (3) Å^3, $K_{T,0} = 102.9$ (28) GPa and $K' = 6.4$ (3). Compression is strongly anisotropic with the a-axes, which lie in the plane of the distorted close-packed layers, approximately 26% more compressible than the c-axis, which is normal to the plane. Structure refinement from single-crystal X-ray intensity data reveals expansion of the structure with Fe substitution, mainly by expansion of M-site octahedra. The short Si2–O6 distance becomes nearly 1% shorter with ~2% Fe substitution for Mg, possibly providing additional rigidity in the c-direction over the Mg end member. K_T obtained for the Fe-bearing sample is ~5.5% greater than reported previously for Fe-free Phase A, despite the larger unit cell volume. This study represents a direct comparison of structure and K_T–ρ relations between two compositions of a F-free dense hydrous magnesium silicate (DHMS) phase, and may help to characterize the effect of Fe substitution on the properties of other DHMS phases from studies of the Fe-free end-members.

Keywords Phase A · High pressure · Hydrous silicates · DHMS · Crystal structure · Bulk modulus

C. M. Holl (✉) · J. R. Smyth
Department of Geological Sciences,
University of Colorado, Boulder, CO, 80309, USA
E-mail: hollc@colorado.edu
Tel.: +1-303-4921696
Fax: +1-303-4922606

M. H. Manghnani · G. M. Amulele · M. Sekar
Hawaii Institute of Geophysics and Planetology,
University of Hawaii, Honolulu, HI, 96822, USA

D. J. Frost
Bayerisches Geoinstitut, Universität Bayreuth,
95440, Bayreuth, Germany

V. B. Prakapenka · G. Shen
Advanced Photon Source, Argonne National Laboratory,
University of Chicago, Chicago, IL, 60637, USA

Introduction

Dense hydrous magnesium silicate minerals have been the subject of increased interest since it has been proposed that these phases may act as a potential carrier of water into the Earth's mantle, and as a reservoir for water in the transition zone in extremely hydrous compositions (Faust and Knittle 1994; Kanzaki 1991). Phase A is one of a group of these phases that lie on the brucite-forsterite join in the MgO–SiO_2–H_2O (MSH) system with the general formula $mMg_2SiO_4 \cdot nMg(OH)_2$. Of these, Phase A is the only phase with $m/n < 1$ and is structurally distinct from the phases with $m/n \geq 1$, which belong to the humite group. Phase A was synthesized by Sclar et al. (1967) and by Ringwood and Major (1967) in studies of the MgO–SiO_2–H_2O system at pressures greater than 5 GPa. Yamamoto and Akimoto (1977) determined the chemical formula (1977) in a study of phase relations in the MSH system at high temperature (500–1,225°C) and pressures up to 7.7 GPa.

Phase A is of interest in studies of the earth's mantle water cycle due to its high water content and its stability at relatively low pressures. Serpentine breaks down to Phase A + clinoenstatite + water at 6.2 GPa and 580°C (Schmidt and Poli 1998) in mantle compositions, although Phase A is known to be stable at relatively low pressures (< 3 GPa) in very Mg-rich environments (Pawley and Wood 1996; Wunder and Schreyer 1997). Owing to its very high water content (approaching 12% by weight), Phase A can coexist with enstatite and chondrodite under mantle conditions, but not with olivine. At higher temperatures Phase A + enstatite breaks down to olivine + water, but this reaction is

stabilized by increased pressure (Schmidt and Poli 1998). Ohtani et al. (2004) place the serpentine-to-Phase A reaction at 200 km depth in a cool subducting slab, and argue that Phase A is stable to 550 km, where hydrous phase B becomes the main vehicle for water transport in the slab. Luth (1995) found that Phase A is not further stabilized by extra components (Al_2O_3, FeO, CaO) to the MSH system, and is therefore not likely to be important for mantle water storage.

Horiuchi et al. (1979) determined the crystal structure of Phase A. The structure is hexagonal (space group $P6_3$) and consists of slightly distorted close-packed layers of O atoms and hydroxyl groups repeating along the c-axis in an ABCB sequence. Cations occur between the layers of anions so that one-half of the available octahedral sites and one-fourteenth of the available tetrahedral sites are filled. Mg occupies one special position on the three-fold axis (M3) and two general positions, M1 and M2. Si occupies two special positions, one each on the three-fold and on the 6_3 axes, so that there is one in each layer of cations. All tetrahedra point in the same direction along c, so that the structure is acentric. The M1 and M2 octahedra each form edge-sharing Mg_3O_{13} groups with equivalent sites. In the M2–M3–Si1 layer these groups are linked by sharing edges with M3 octahedra; the groups in the M1–Si2 layer are isolated. Edge sharing also occurs between Si2 tetrahedra and M2 octahedra between layers. The structure differs from the humite group minerals in that no intra-layer edge sharing between octahedral and tetrahedral sites exists (Horiuchi et al. 1979) in Phase A, and chains of Mg octahedra that are thought to control compressibility in humite group minerals (Faust and Knittle 1994) are absent.

Because of this phase's stability at relatively low pressures and high water contents (>11 wt%), it is a potential breakdown product of serpentine, which makes it particularly interesting as a possible carrier of water in subduction zones. Its equation of state therefore has been of particular interest. Previous compression studies of Fe-free Phase A report a range of values for bulk moduli. Kudoh et al. (2002) obtained a value of $K_0 = 105$ GPa (K' fixed at four) from high-pressure powder diffraction using synchrotron radiation. Kuribayashi et al. (1999) obtained $K_0 = 105$ (4) and $K' = 4.4$ (11) from single-crystal cell parameter measurements up to 11 GPa. Crichton and Ross (2002) made high-precision single-crystal unit cell measurements using quartz cell volume as a pressure standard (Angel et al. 1997). They obtained $K_0 = 97.5 \pm 0.4$ GPa and $K' = 5.97 \pm 0.14$, a significantly lower bulk modulus than from previous studies. However, their reported K′ was significantly higher. They also refitted their data to a Birch-Murnaghan equation of state curve using fixed $K' = 4.4$ from Kuribayashi et al. (1999) and obtained similar values for K_0, indicating that the Crichton and Ross and the Kuribayashi et al. data sets are similar and the difference in values are due to weighting schemes and the covariance of the parameters K and K'.

In order to determine the effects of Fe substitution on the structure and equation of state of an iron-bearing, fluorine-free DHMS phase, we have conducted a study of the equation of state encompassing the entire pressure stability range of Fe-bearing Phase A by synchrotron powder diffraction and a structure refinement at ambient pressure and temperature. If Phase A exists in subducting slabs as a breakdown product of serpentinized mantle material with peridotite composition, it would be expected to contain close to typical mantle Fe/(Fe(Mg) values of 0.08–0.12. Though static compression studies on natural DHMS phases have been performed, the interpretation of those results is complicated by fluorine substitution for hydroxyl. By studying a sample with this particular composition we hope to further understand the effect of iron substitution on the properties of DHMS phases.

Experimental

Synthesis

Fe-bearing Phase A was synthesized in the 5,000-ton multi-anvil press at Bayerisches Geoinstitut, Bayreuth, Germany. An outer 3.5 mm welded Pt capsule contained two separate 1.6 mm diameter welded Pt inner capsules in a matrix of brucite to maintain H activity. The inner capsule contained a 1 mm cube single-crystal of San Carlos olivine, plus a mixture of brucite and forsterite. The inner capsules also contained small amount of a Re–ReO_2 oxygen buffer to maintain the iron in the ferrous state. The run was made in an 18 mm sintered MgO octahedron in 5,000 ton press using 54 mm WC cubes with 8 mm corner truncations. The nominal pressure was 12 GPa at 1,200°C with a heat cycle duration of 180 min.

The original objective of the experiment was to hydrate the San Carlos olivine, but rupture of the one of the inner capsules exposed the San Carlos olivine to excess brucite, with which it reacted to form Phase A. The only phases identified in the capsule were Phase A and brucite. The Phase A crystals were up to 0.25 mm in diameter and light tan in color. Electron microprobe chemical analyses of the Phase A crystals, with H_2O determined by difference, give the formula $Mg_{6.85}Fe_{0.14}Si_{2.00}O_8(OH)_6$.

Powder diffraction

Crystals were ground in an agate mortar to powder grain size of 1–3 μm and loaded in a four-pin, piston-cylinder 300 μm culet diamond anvil cell with tungsten carbide seats and a 60° optical aperture. Gaskets were stainless steel pre-indented to 35 μm thickness and a sample chamber drilled to 130 μm diameter. Several small (<30 μm) ruby crystal chips were included as an independent pressure standard. Silicone oil was used as

the pressure medium in order to minimize interference of pressure medium diffraction peaks with the pattern at high pressure. Powder X-ray diffraction data up to 33 GPa were collected at beamline 13-BM-D at GSE-CARS, Advanced Photon Source, Argonne National Laboratory. Incident synchrotron radiation was monochromatized to 0.3344 Å. The diffraction pattern was captured on a MAR345 imaging plate and integrated using the software package FIT2D (Hammersley et al. 1996). Unit cell parameters were refined using a Rietveld fit in the program GSAS (Larson and Von Dreele 2000). Pressure measurements were obtained using the shift in ruby fluorescence spectral line (Mao et al. 1986). Uncertainties in the pressure were estimated from the scatter in values from repeated measurements. Cell parameters and pressures are reported in Table 1 and diffraction patterns stacked by pressure are given in Fig. 1. Equation-of-state calculations were performed using the program EOSFIT 4.2 (Angel 1998). Weights were assigned to the individual data based on volume ESDs provided by the refinement program, and the estimated pressure uncertainties.

Single crystal diffraction

The unit cell parameters were determined from centering of 10 reflections in each of 8 octants on a Huber four circle diffractometer running the instrument control code SINGLE04 (R. J. Angel, personal communication.) The cell parameters thus determined are $a = 7.8678$ (4) Å, $c = 9.5771$ (5) Å, and $V = 513.43$ (4) Å^3. The density of the sample calculated from the above formula and these cell parameters is 2.979 g/cm^3. The crystal structure was refined from an intensity data set measured using a Bruker APEX2 CCD detector on a Bruker diffractometer equipped with a Cu sealed tube X-ray source. The data set consists of 2,118 measured intensities of which 545 are unique. Data were corrected for absorption, and equivalent intensities were merged to give an internal R of 0.020. After application of a significant isotropic extinction correction, the full-matrix least-squares atom parameter refinement (Sheldrick 1997) converged to a final $R(F)$ of 0.029 for all intensities. Final atom parameters are given in Table 2. Nearest neighbor atomic distances and coordination polyhedron parameters are given in Table 3.

Table 1 Unit cell parameters for Fe-bearing Phase A at pressure by synchrotron powder diffraction

Pressure (*Gpa*)	*a* (Å)	*c* (Å)	Vol. (Å^3)
0.0001	7.8667 (6)	9.5651 (17)	512.62 (7)
1.0 (1)	7.8316 (4)	9.5300 (13)	506.21 (6)
3.2 (1)	7.7897 (4)	9.4933 (12)	498.87 (5)
5.5 (1)	7.7310 (6)	9.4320 (19)	488.20 (7)
7.4 (1)	7.6994 (8)	9.392 (2)	482.15 (9)
9.5 (1)	7.6621 (7)	9.364 (2)	476.11 (7)
11.3 (2)	7.6329 (8)	9.350 (2)	471.78 (7)
13.4 (2)	7.5991 (6)	9.3325 (18)	466.71 (6)
14.4 (2)	7.5785 (8)	9.312 (2)	463.17 (8)
16.7 (3)	7.5383 (10)	9.293 (3)	457.35 (11)
19.3 (3)	7.5199 (13)	9.249 (4)	452.94 (13)
21.9 (4)	7.4873 (10)	9.221 (3)	447.67 (11)
24.5 (4)	7.4431 (14)	9.192 (4)	441.03 (15)
26.4 (5)	7.4287 (16)	9.180 (5)	438.75 (16)
28.5 (5)	7.4079 (17)	9.138 (5)	434.26 (18)
31.3 (6)	7.3789 (15)	9.112 (5)	429.69 (16)
33.2 (6)	7.3512 (17)	9.091 (6)	425.44 (20)

Errors on pressure measurements are estimated from multiple measurements per pressure interval

Results

Crystal structure

Cell parameters obtained by single-crystal X-ray diffraction for Fe-bearing Phase A are $a = 7.8678$ (4) Å, $c = 9.5771$ (5) Å, and $V = 513.43$ (4) Å^3. We attribute the discrepancy between the volumes measured by single crystal X-ray diffraction (SXD) and by powder synchrotron diffraction ($V_0 = 512.62$ Å^3) to different calibration methods between the instruments. The initial cell volume V_0 determined by SXD is 0.26 and 0.32% larger than those reported for pure $Mg_7Si_2H_6O_{14}$ by Horiuchi et al. (1979) and Crichton and Ross (2002), respectively. The a-axis is 0.13 and 0.11% larger, and c is 0.06 and 0.04% larger than reported by the two previous studies. The volumes of the M1, M2, and M3 octahedra increase by 0.54, 0.47, and 0.46%, respectively, over the Fe-free structure. The O2–O3 and O4–O3 polyhedral edges are 0.5 and 0.4% greater in Fe-bearing Phase A than in pure-Mg Phase A structure. These edges approximately correspond to the directions of the O2–H and O4–H hydroxyl bonds and the H–O3 hydrogen bonds. The degree of Fe substitution was determined by modeling Fe and Mg in each site and allowing the occupancy factors of each to refine while constraining the sum to equal full site occupancy. The Fe/(Fe(Mg) ratio is 1.9, 1.7, and 2.6% for M1, M2, and M3, respectively.

Calculations of Madelung site potentials based on assumed point charges and distances in the structure were made (Smyth 1989) and are presented in Table 2. Point charges were nominal valences, and hydroxyl was modeled with point charges of −1 at O2 and O4. There is no apparent evidence for Fe ordering based on the octahedral site potentials. The potential at M3 is slightly lower than at M1 or M2 despite M3 being the smallest octahedron in the structure. This is consistent with M3 not being part of the Mg_3O_{13} groups, but rather M3 is bonded to six hydroxyls and does not share any oxygen with silicate tetrahedra.

Compression

Unit cell parameters at pressure are presented in Table 1, with volumetric and axial strains plotted in Fig. 2. The value for ambient pressure volume is lower from

Table 2 Atom position, occupancy, and displacement parameters for Phase A at ambient pressure

ATOM	x	y	z	s.o.f.	U_{11}	U_{22}	U_{33}	U_{23}	U_{13}	U_{12}	U_{eq}	E.S.P.(V)
M1	0.37273(17)	0.45537(15)	0.3843(7)	Mg: 0.981(8) Fe: 0.019(8)	0.0028(6)	0.0040(6)	0.0067(9)	−0.0005(5)	−0.0024(5)	0.0017(4)	0.0045(5)	−22.4
M2	0.22477(15)	0.24370(14)	0.1120(6)	Mg: 0.983(7) Fe: 0.017(7)	0.0026(6)	0.0024(6)	0.0048(8)	−0.0003(4)	−0.0010(5)	0.0007(4)	0.0035(5)	−22.7
M3	1/3	2/3	0.1020(7)	Mg: 0.325(6) Fe: 0.009(6)	0.0129(8)	0.0129(8)	0.0139(11)	0	0	0.0065(4)	0.0132(7)	−19.9
Si1	2/3	1/3	0.1730(6)	1/3	0.0017(6)	0.0018(6)	0.0044(9)	0	0	0.0009(3)	0.0026(5)	−49.0
Si2	0	0	0.4007(6)	1/3	0.0042(5)	0.0042(5)	0.0040(10)	0	0	0.0021(3)	0.0041(5)	−46.7
O1	0.2013(3)	0.0276(3)	−0.0230(5)	1	0.0027(11)	0.0024(12)	0.0074(17)	0.0014(10) 0.0047(12)	0.0003(10) 0.0046(6)	27.3		
O2	0.4761(4)	0.0988(3)	0.4842(5)	1	0.0039(12)	0.0038(12)	0.0091(20)	−0.0013(9) 0.0000(10)	0.0016(9)	0.0057(7)	12.0	
O3	0.4541(3)	0.2936(3)	0.2328(8)	1	0.0057(11)	0.0077(12)	0.0056(12)	−0.0018(11)	0.0044(16)	0.0034(10)	0.0063(6)	24.6
O4	0.1703(4)	0.4364(3)	0.2394(8)	1	0.0063(12)	0.0046(10)	0.0056(14)	0.0012(11)	−0.0017(15)	0.0019(10)	0.0059(6)	13.0
O5	2/3	1/3	0	1/3	0.0024(13)	0.0024(13)	0.0060(24)	0	0	0.0012(6)	0.0036(10)	27.9
O6	0	0	0.2329(10)	1/3	0.0048(12)	0.0048(12)	0.0076(26)	0	0	0.0024(6)	0.0057(10)	27.3

The electrostatic site potentials calculated are also tabulated from a point charge model (Smyth 1989)

synchrotron powder diffraction than from SXD due to calibration methods for the two instruments. P–V data used to obtain equation of state are obtained entirely from synchrotron powder diffraction. Fitting the P–V data to a third order Birch-Murnaghan isothermal equation of state curve gives $V_0 = 512.3$ (3) Å^3, $K_{T,0} = 102.9$ (28) GPa and $K' = 6.4$ (3). P–V data were plotted as Birch-normalized-pressure versus Euler strain (Fig. 3). Plotting P–V data in this manner will visually show whether high order terms in the Birch-Murnaghan EoS are important. A horizontal linear best-fit curve indicates that K' is close to the assumed value of four for a normal close-packed oxygen array, and that a second-order fit is sufficient. Our data show a clear positive slope, indicating a third-order fit with $K' > 4$ is required. From the zero-pressure intercept and the slope, we obtain $K_{T,0} = 101.1$ (14) GPa and $K' = 6.6$ (1). Deviation from the P–V derived values is probably due to high uncertainties in V_0 and low-P values. Linear moduli and pressure derivatives were calculated from axial lengths and pressure data using the program EoSFit 4.2 (Angel 1998). For the a-axis, a third-order Birch-Murnaghan fit gave $a_0 = 7.865$ (37) Å, $K_a = 97.3$ (3) GPa, $K_a' = 5.3$ (3). The c-axis appears to show an abrupt stiffening between 8 and 10 GPa (Fig. 2b). This may indicate a real change in compression mechanism or a strain limit reached in the compression-controlling Si2 layers, or it could be attributed to non-hydrostatic stress from stiffening of the pressure-transmitting medium. Noticeable broadening of diffraction peaks is not apparent until pressures >15 GPa are reached, suggesting that the medium maintained near-hydrostatic conditions until this point. For the c-axis, it was necessary to constrain the fit by fixing K′ to the value of 7.5 (Crichton and Ross 2002). The third-order Birch-Murnaghan fit gives $c_0 = 9.56$ (12) Å, $K_c = 131$ (4) GPa. However, if the fit for c is recalculated using only data to ~10 GPa, the value for K_c' is similar to that from Crichton and Ross (2002), albeit with large uncertainties due to low precision data combined with a smaller number of data points. Compression is strongly anisotropic with the a-axis direction, parallel to the oxygen layers, approximately 26% more compressible than the c-axis direction, perpendicular to the layers. Data reported by Crichton and Ross (2002) shows the a-axis being approximately 23% more compressible, suggesting that Fe-substitution increases compression anisotropy in Phase A.

Discussion

The expansion of this structure relative to the pure-Mg Phase A is consistent with its Fe content which may also play a role in the apparent stiffening of the structure relative to pure-Mg Phase A. The crystal structure refinement shows no significant ordering of Fe based on the X-ray scattering of the three octahedral sites and on the polyhedral volumes relative to the pure-Mg Phase A. This is consistent with the rapid quench from 1,250°C in

Table 3 Selected nearest neighbor distances and coordination polyhedral parameters for Phase A at ambient pressure

Mg1–O1	2.0271	Mg2–O1	2.0702	Mg3–O2	2.0402
–O2	2.0042	–O1	2.1972	–O2	2.0402
–O3	2.2256	–O2	2.0224	–O2	2.0402
–O4	2.0616	–O3	2.0107	–O4	2.0829
–O4	2.3868	–O4	2.1504	–O4	2.0829
–O5	2.1463	–O6	2.1811	–O4	2.0829
Avg. Mg1–O	2.1419	2.1053	2.0615		
Poly. Vol.	12.784	12.116	11.590		
Ang. Var.	53.64	62.72	18.63		
O.Q.E.	1.020	1.019	1.005		
Si1–O3(3)	1.6438	Si2–O1(3)	1.6576		
–O5(1)	1.6573	–O6(1)	1.6075		
Avg. Si–O	1.6572	1.6451			
Poly. Vol.	2.293	2.241			
Ang. Var.	1.043	60.15			
T.Q.E.	1.000	1.013			

the synthesis and close similarity in cation site sizes. All octahedral sites have a greater volume compared to the pure-Mg structure, and calculated occupancy factors show all sites to be near capacity based on Mg ion scattering. Differences in bond lengths between Fe-bearing and Fe-free Phase A is illustrated in Fig. 4. The Si2 tetrahedron increases in volume and average bond length, but shows a distinct shortening of the Si2–O6 bond, from 1.623 to 1.608 Å. This bond is the shortest cation-oxygen distance in the structure, and is parallel to the *c*-axis. The O1–O1 edges are shared across layers by the Si2 and Mg2 sites, and at 2.577 Å are the shortest polyhedral edges in the structure. The Si1–O5 bond is shorter in the Fe-bearing structure, 1.667 Å compared to 1.657 Å in the pure-Mg structure. The silicate tetrahedra, and in particular, the unique Si–O bond parallel to the stacking direction, would appear to control compression in Phase A. Kuribayashi et al. (2003) report little change in Si–O bond lengths up to 9.4 GPa. However, we observe a ~2% increase in volume and increases in angle variance and quadratic elongation (factors describing distortion of intra-polyhedral angles and edge lengths from an ideal polyhedron) for Si2. Expansion of the octahedral sites and void spaces with the addition of iron distorts the tetrahedral sites, elongating the bonds roughly parallel to the layers and shortening the bonds perpendicular to the layers. This distortion is more pronounced in the Si2 tetrahedra, which share edges with the octahedra in the adjacent layer, than in the Si1 tetrahedra, which share only corners. Therefore, we would expect the M1 layers containing the Si2 tetrahedra to be less compressible in the *c*-direction than the M2M3 layers. Since Mg octahedral chains analogous to those in the humite group are absent in Phase A, the tetrahedral sites may also be controlling the compressibility of the *a*-direction, despite having only 1/16 of tetrahedral sites filled.

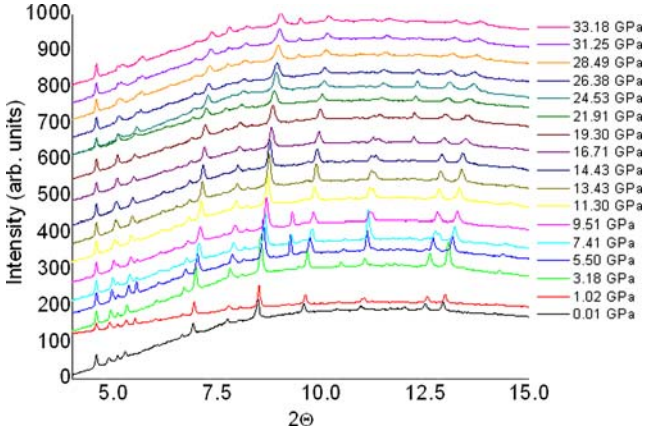

Fig. 1 Stacked powder diffraction patterns of Phase A at various pressures. The figure shows the regular compression behavior of the material. Anomalous peaks are attributed to the ruby internal pressure standard

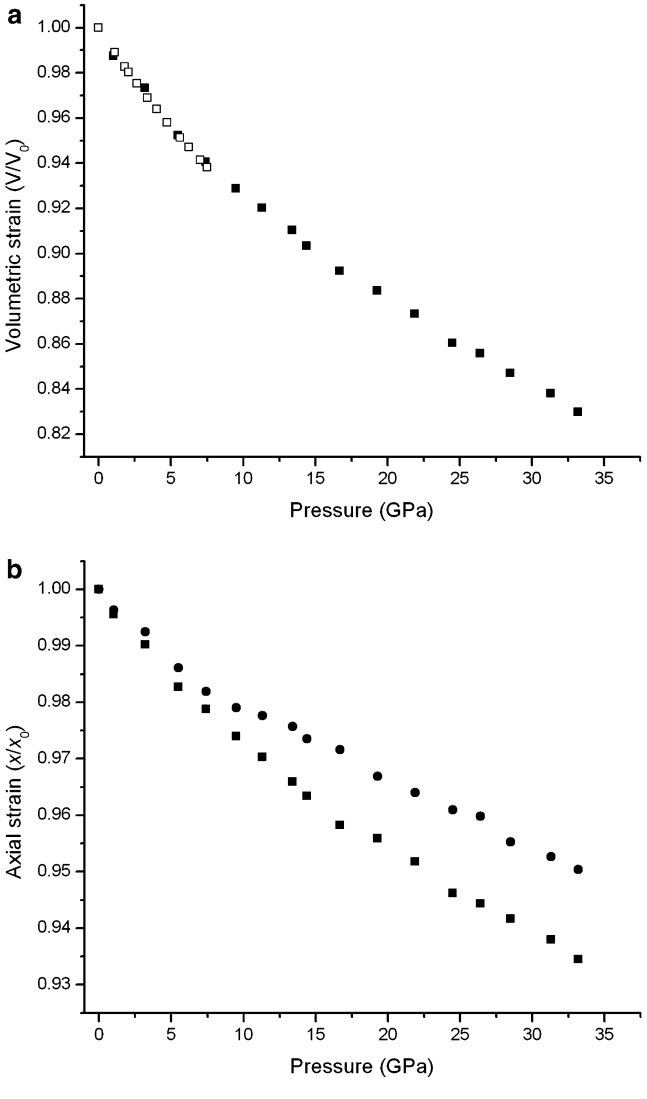

Fig. 2 Volumetric **a** and axial **b** strain plots for Fe-bearing Phase A. For **a**, *open squares* represent data from Crichton and Ross (2002) for Fe-free Phase A, *closed squares* are from the current study

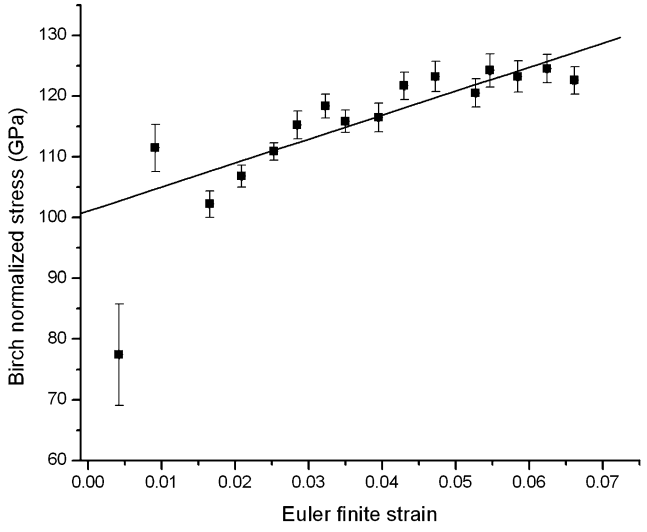

Fig. 3 Plot of Birch normalized stress (F) against Euler finite strain (f_E) for Phase A compression. Slope of the linear regression curve is equal to $3K_T(K'-4)/2$. EoS terms from the intercept and slope of the linear regression curve are $K_T = 101.1(14)$ GPa and $K' = 6.6(1)$. Scatter is likely due to error in the pressure measurements of the P–V data and uncertainty in V_0

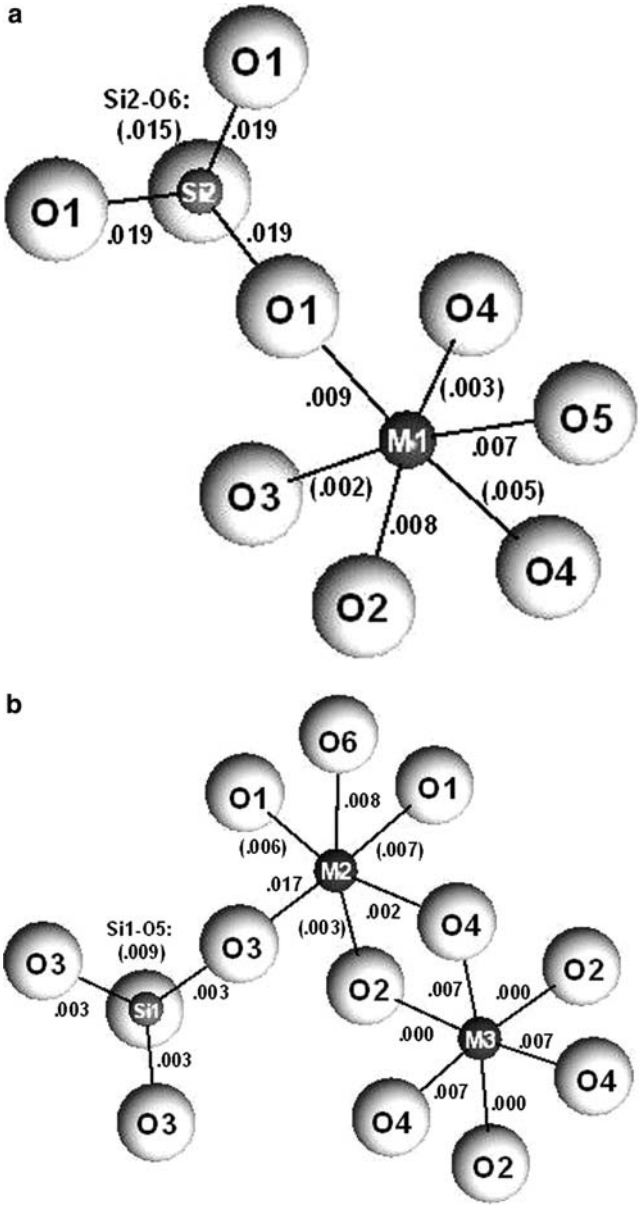

Fig. 4 Absolute difference in bond lengths in Å between Fe-bearing Phase A structure and the Fe-free structure of Horiuchi et al. (1979) in **a** M1 layer and **b** M2M3 layer. Values in parentheses indicate a negative change in bond length (shorter bond in Fe-bearing structure). The structure is hexagonal (space group $P6_3$) with the O5 lying on the rotation axis. View is approximately parallel to (0 0 1). Figure drawn using XtalDraw (Downs et al. 2001)

Refinement of the Fe-bearing structure shows a possible slight preference for Fe occupancy in the M3 site, although the presence of Fe-ordering could not be determined unequivocally. M3 is the smallest of the normally occupied octahedral sites, but it is bonded to six hydroxyls and may better accommodate Fe. Rapid quenching of the ruptured capsule may have preserved disorder in the sample. Structure refinement and electron microprobe analysis both indicate a nearly ideal chemical formula, consistent with a fully disordered sample.

Because previous researchers reported different parameters that represented essentially the same EoS, care was taken to determine whether our higher K_T represented true behavior or was due to fitting procedures. Depending on the weighting scheme implemented, a range of values was obtained for K_T, from ~102 to ~108 GPa, all higher than previous studies when adjusted for covariance of the K and K' parameters and consistent with the covariance. The final values reported represent the EoS with the most favorable statistical fit and a weighting scheme judged to be reasonable. The bulk modulus, $K_{T,0} = 102.9$ (28) GPa, is 5.5% higher than the value from Crichton and Ross (2002), but in agreement within combined errors of the value of Kuribayashi et al. (1999). The value for K' is higher than the value of Crichton and Ross (2002), suggesting that the difference in the values for K_0 is not simply due to fitting and weighting procedures. Refitting the data set from Kuribayashi et al. (2003) using a fixed value of $K' = 5.97$ determined by Crichton and Ross (2002) gives $K_{T,0} = 98.1$ (9) GPa with only a slight increase in weighted chi-squared value. Therefore, the two data sets produce similar results and the differences in the reported numbers may be due to differences in weighting schemes. For comparison with the previous results, we refit our entire data set and fixed K' to the values from those studies. Fixing $K' = 5.97$ (Crichton and Ross 2002) yields $K_{T,0} = 105.8$ (13) GPa, and fixing $K' = 4.4$ (Kuribayashi et al. 2003) yields $K_{T,0} = 116.8$ (21) GPa, confirming that the higher K_T observed for the Fe-bearing Phase A is not due to differences in the data fitting procedure.

Elasticity determination by Brillouin scattering on the same material gives $K_S = 106$ GPa (Sanchez-Valle et al. 2005). K_T can be roughly estimated using the relation $K_S = K_T(1 + \alpha\gamma T)$ with $\alpha = 4.9(2)(\times 10^{-5}\,^{\circ}C^{-1}$

(Pawley et al. 1995) and γ similar to the value for forsterite (~1.2), giving K_T approximately 104.2 GPa. The linear moduli values obtained, $K_a = 97.3$ (3) GPa and $K_c = 131$ (3) GPa, are ~8 and ~12% higher than those from Crichton and Ross (2002). Calculated K_a' was consistent with that study, and K_c' was constrained to be consistent so K_c could be compared. *a*-axis lengthening in the Fe-bearing phase is over four times the *c*-axis lengthening relative to the Fe-free phase, whereas M site expansion is nearly uniform, consistent with a greater increase in K_c than in K_a. The axial ratio varies as

$$c/a = 1.255(9) + 1.0(2) \times 10^{-3} \cdot P - 1.1 \times 10^{-5} \cdot P^2$$

over the entire pressure range studied. The curvature of this relation is lower than that found by Crichton and Ross (2002) for Fe-free Phase A, but initial c/a for the Fe-bearing phase is sufficiently lower so that it should remain less than that for the Fe-free sample throughout the Phase A pressure stability range.

K_T is plotted against ρ for DHMS phases along the forsterite-brucite join for which isothermal bulk modulus data are available in Fig. 5. Ross and Crichton (2001) report a simple linear correlation between density and isothermal bulk modulus of DHMS phases:

$$K_T = 97(6) \times \rho - 186(17)\ \text{GPa}$$

This relationship accurately predicts the bulk modulus for this particular composition of Fe-bearing Phase A [$K_{T,calc} = 103$ (1) GPa, $K_{T,obs} = 102.9$ (28) GPa]. For Phase A with an approximated mantle cation ratio Fe/(Fe + Mg) = 0.92, the equation predicts $K_T = 111$ (2) GPa, assuming no further volume expansion with additional Fe substitution. Since the K_T-density relation given by Ross and Crichton (2001) appears to hold for Fe-bearing Phase A, it may be useful for predicting behavior of naturally occurring DHMS phases, which are certain to contain some amount of Fe for Mg. However, the observed increase in K_T with 2% Fe substitution (~5.5%) is greater than the predicted increase (~2.2%) from the above equation, suggesting that Fe may enhance the stiffening of the structure beyond the effect of density.

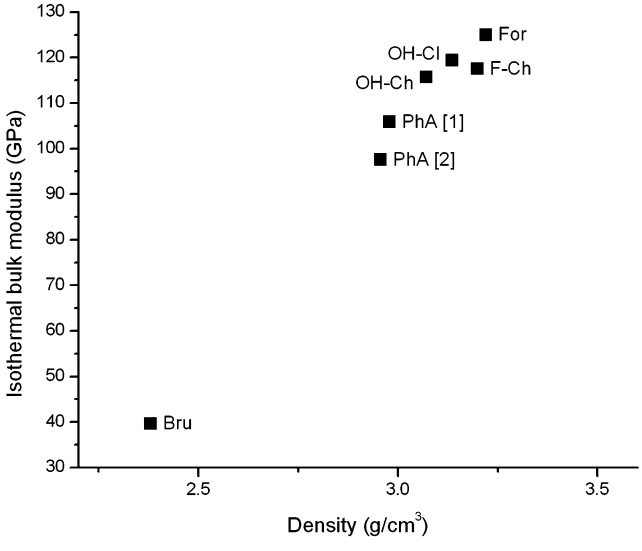

Fig. 5 Plot of K_T against density for DHMS phases along the forsterite-brucite join, after Ross and Crichton (2001). PhA [1]: Fe-bearing Phase A, this study; PhA [2]: Fe-free Phase A, Crichton and Ross (2002); OH-Ch: synthetic hydroxylchondrodite, Ross and Crichton (2001); OH-Cl: synthetic hydroxylchondrodite, Ross and Crichton (2001); F-Ch: natural F-bearing chondrodite, Friedrich et al. (2002); For: synthetic forsterite, Downs et al. (1996); Bru: brucite, Xia et al. (1998)

Friedrich et al. (2002) studied the compression of a natural fluorine-bearing chondrodite, and suggested that F substitution for OH in chondrodite increases the bulk modulus of the material. In F-free Phase A, we observe a ~2.7% increase in K_T per 1% Fe/(Fe(Mg). Friedrich et al. (2002) report ~1.5% increase in K_T for natural chondrodite with OH/(F + OH) = 0.44 compared to pure synthetic hydroxylchondrodite (Ross and Crichton 2001), with this increase attributed to F substitution. However, the natural chondrodite studied by Friedrich et al. contained ~5.6% Fe/M_{total}, and they obtained $K_T = 117.5$ (4) GPa for the material. Using the equation from Ross and Crichton (2001), the predicted K_T for this natural chondrodite is 124 (2) GPa. If F substitution in DHMS phases does indeed increase bulk modulus, then there is probably a mechanism with a competing effect, possibly substitution of Mg by excess H or trivalent cations forcing vacancy of normally occupied sites. As naturally occurring Phase A is likely to contain these defects to some degree, the value of the K_T-density relationship may be limited for predicting its compressional behavior. In addition, Phase A is structurally distinct from other DHMS phases on the Fo-Br join, and while Phase A appears to follow the K_T-density correlation among DHMS phases, it violates correlation between K_T and packing index, and K_T between filling factors (Kuribayashi et al. 2003). Therefore, the effect of Fe on K_T in Phase A may not necessarily be a valid proxy for the humite group minerals due to differing compression mechanisms.

In summary, we have synthesized and refined the crystal structure of an iron-bearing Phase A. The structure shows a uniform expansion relative to previous studies of pure-Mg Phase A and no ordering of the Fe among the three distinct octahedra is observed. We have conducted an isothermal compression study of Phase A by synchrotron powder diffraction to 33 GPa. Fitting high-pressure cell parameters to a third order Birch-Murnaghan equation of state, we obtain a significantly higher K_T that cannot be entirely explained by differences in fitting procedures. This value is approximately ~2.7% greater per 1% Fe/(Fe(Mg) than for Fe-free Phase A, and consistent with the K_T-ρ systematics of DHMS phases as defined by Ross and Crichton (2001) for low Fe contents.

Acknowledgements This research was supported by the U.S. National Science Foundation grants EAR 03-36611 to JRS, EAR 00-74285 and Army/TARDEC Contract DAAE07-01-C-L055 to

MHM, the Bayerisches Geoinstitut Visitors Program, and the Alexander von Humboldt Foundation. Portions of this work were performed at GeoSoilEnviroCARS (Sector 13), Advanced Photon Source (APS), Argonne National Laboratory. GeoSoilEnviroCARS is supported by the National Science Foundation–Earth Sciences (EAR-0217473), Department of Energy–Geosciences (DE-FG02-94ER14466) and the State of Illinois. Use of the APS was supported by the U.S. Department of Energy, Basic Energy Sciences, Office of Energy Research, under Contract No. W-31-109-Eng-38. The authors would like to thank W. A. Crichton and an anonymous reviewer for their constructive comments.

References

Angel RJ (1998) EOSFIT 4.2: program for EoS calculations

Angel RJ, Miletich R, Finger LW (1997) The use of quartz as an internal pressure standard in high-pressure crystallography. J Appl Cryst 30:461–466

Crichton WA, Ross NL (2002) Equation of state of dense hydrous magnesium silicate Phase A, $Mg_7Si_2O_8(OH)_6$. Am Mineral 87:333–338

Downs RT, Zha C-S, Duffy TS, Finger LW (1996) The equation of state of forsterite to 17.2 GPa and effects of pressure media. Am Mineral 81:51–55

Downs RT, Sinnaswamy K, Bartolmehs K (2001) XtalDraw: program to draw crystal structures and molecules. Beta Version, August 1, 2001. University of Arizona

Faust J, Knittle E (1994) Static compression of chondrodite: Implications for water in the upper mantle. Geophys Res Lett 21:1935–1938

Friedrich A, Lager GA, Ulmer P, Kunz M, Marshall WG (2002) High-pressure single-crystal X-ray and powder neutron study of F,OH/OD-chondrodite: compressibility, structure, and hydrogen bonding. Am Mineral 87:931–939

Hammersley AP, Svensson SO, Hanfland M, Fitch AN, Hausermann D (1996) Two-dimensional detector software: from real detector to idealised image or two-theta scan. High Press Res 14:235–242

Horiuchi H, Morimoto N, Yamamoto K, Akimoto S (1979) Crystal structure of $2Mg_2SiO_4.3Mg(OH)_2$, a new high-pressure structure type. Am Mineral 64:593–598

Kanzaki M (1991) Stability of hydrous magnesium silicates in the mantle transition zone. Phys Earth Planet Int 66:307–312

Kudoh Y, Kuribayashi T, Kagi H, Sasaki S, Tanaka M (2002) High-pressure structural study of phase-A, $Mg_7Si_2H_6O_{14}$ using synchrotron radiation. J Phys Cond Matt 14:10491–10495

Kuribayashi T, Kudoh Y, Kagi H (1999) High pressure X-ray diffraction study on Phase A, $Mg_7Si_2H_6O_{14}$, up to 11.2 GPa. EOS, Trans AGU 80:F938

Kuribayashi T, Kudoh Y, Kagi H (2003) Compressibility of Phase A, $Mg_7Si_2H_6O_{14}$ up to 11.2 GPa. J Min Pet Sci 98:215–234

Larson, AC, Von Dreele, RB (2000) General structure analysis system. Los Alamos unclassified report LAUR 86–748, Los Alamos National Laboratory, pp 231

Luth RW (1995) Is Phase A relevant to the Earth's mantle? Geochim Cosmochim Acta 59:679–682

Mao HK, Xu J, Bell PM (1986) Calibration of the ruby pressure gauge to 800 kbar under quasi-hydrostatic conditions. J Geophys Res 91:4673

Ohtani E, Litasov K, Hosoya T, Kubo T, Kondo T (2004) Water transport into the deep mantle and formation of a hydrous transition zone. Phys Earth Planet Int 143–144:255–269

Pawley AR, Wood BJ (1996) The low-pressure stability of Phase A, $Mg_7Si_2O_8(OH)_6$. Contr Min Pet 124:90–97

Pawley RP, Redfern SAT, Wood BJ (1995) Thermal expansivities and compressibilities of hydrous phases in the system MgO–SiO_2–H_2O: talc, Phase A and 10-Å phase. Contr Min Pet 122:301–307

Ringwood AE, Major A (1967) High-pressure reconnaissance investigations in the system MgO–SiO_2–H_2O. Earth Planet Sci Lett 2:130–133

Ross NL, Crichton WA (2001) Compression of synthetic hydroxylclinohumite [Mg9Si4O16(OH)2] and hydroxylchondrodite [$Mg_5Si_2O_8(OH)_2$]. Am Mineral 86:990–996

Sanchez-Valle C, Sinogeikin SV, Smyth JR, Bass JD (2005) Single-crystal elastic properties of Phase A to 12 GPa. Geological Society of America Abstracts with Programs 37:285

Schmidt MW, Poli S (1998) Experimentally based water budgets for dehydrating slabs and consequences for arc magma generation. Earth Planet Sci Lett 163:361–379

Sclar CB, Carrison LC, Stewart OM (1967) High-pressure synthesis of a new hydroxylated pyroxene in the system MgO–SiO_2–H_2O. EOS Trans AGU 48:226

Sheldrick GM (1997) SHELXL-97–a program for crystal structure refinement. University of Goettingen, Germany, pp 97–2

Smyth JR (1989) Electrostatic characterization of oxygen sites in minerals. Geochim Cosmochim Acta 53:1101–1110

Wunder B, Schreyer W (1997) Antigorite: high pressure stability in the system MgO–SiO_2–H_2O. Lithos 41:213–227

Xia X, Weidner DJ, Zhao H (1998) Equation of state of brucite: Single-crystal Brillouin spectroscopy study and polycrystalline pressure-volume-temperature measurement. Am Mineral 83:68–74

Yamamoto K, Akimoto S (1974) High-pressure and high-temperature investigation in the system MgO–SiO_2–H_2O. J Solid State Chem 9:187–195

Yamamoto K, Akimoto S (1977) The system MgO–SiO_2–H_2O at high pressure and temperatures—stability field for hydroxyl-chondrodite, hydroxyl-clinohumite, and 10 Å-phase. Am J Sci 277:288–312